

3'UTR length-dependent control of SynGAP isoform $\alpha 2$ mRNA by FUS and ELAV-like proteins promotes dendritic spine maturation and cognitive function

Satoshi Yokoi¹⁾, Tsuyoshi Udagawa^{1) 2) #}, Yusuke Fujioka¹⁾, Daiyu Honda¹⁾, Haruo Okado³⁾, Hirohisa Watanabe¹⁾⁴⁾, Masahisa Katsuno¹⁾, Shinsuke Ishigaki^{1)5)#}, Gen Sobue¹⁾

4) #

1) Department of Neurology, Nagoya University Graduate School of Medicine, Nagoya, Aichi 466-8550, Japan

2) Graduate School of Pharmaceutical Sciences, Tohoku University, Sendai, Miyagi 980-8578, Japan

3) Department of Brain Development and Neural Regeneration, Tokyo Metropolitan Institute of Medical Science, Setagaya-ku, Tokyo, 156-8506, Japan

4) Research Division of Dementia and Neurodegenerative Disease, Nagoya University Graduate School of Medicine, Nagoya, Aichi 466-8550, Japan

5) Department of Therapeutics for Intractable Neurological Disorders, Nagoya University Graduate School of Medicine, Nagoya, Aichi 466-8550, Japan

Correspondence and requests for materials should be addressed to Gen Sobue (sobueg@med.nagoya-u.ac.jp), Tsuyoshi Udagawa (udagawa17@gmail.com), or Shinsuke Ishigaki (ishigaki-ns@umin.net). Lead contact; Gen Sobue

Abstract

FUS is an RNA-binding protein associated with frontotemporal lobar degeneration (FTLD) and amyotrophic lateral sclerosis (ALS). Previous reports have demonstrated intrinsic roles of FUS in synaptic function. However, the mechanism underlying FUS's regulation of synaptic morphology has remained unclear. We found that reduced mature spines after FUS depletion was associated with the internalization of PSD-95 within the dendritic shaft. Mass spectrometry of PSD-95-interacting proteins identified SynGAP, whose expression decreased after FUS depletion. Moreover, FUS and the ELAV-like proteins ELAVL4 and ELAVL1 control SynGAP mRNA stability in a 3'UTR length-dependent manner, resulting in the stable expression of the alternatively spliced SynGAP isoform $\alpha 2$. Finally, abnormal spine maturation and FTLD-like behavioral deficits in FUS knockout mice were ameliorated by SynGAP $\alpha 2$. Our findings establish an important link between FUS and ELAVL proteins for mRNA stability control and indicate that this mechanism is crucial for the maintenance of synaptic morphology and cognitive function.

Introduction

FUS/TLS is an RNA-binding protein with a genetic and pathologic relationship to frontotemporal lobar degeneration (FTLD) and amyotrophic lateral sclerosis (ALS) (Kwiatkowski et al., 2009; Neumann et al., 2009; Seelaar et al., 2011). FUS is mislocalized from the nucleus to cytoplasm and exhibits aggregate formation in FTLD/ALS (Mackenzie et al., 2011; Neumann et al., 2009). A gain of toxic function and/or loss of function of FUS have been hypothesized as pathogenic mechanisms. FUS has various roles in RNA metabolism, including functions related to alternative splicing (Lagier-Tourenne et al., 2012; Ishigaki et al., 2017), transcription (Tan and Manley, 2010; Masuda et al., 2015), mRNA transport (Fujii et al., 2005), mRNA stability (Kapeli et al., 2016; Udagawa et al., 2015), translation (Yasuda et al., 2013), and miRNA processing (Morlando et al., 2012). Disruption of these functions may correspond to the pathogenesis of FTLD/ALS (Ling et al., 2013).

The regulation of mRNA stability via deadenylation is a crucial mechanism in RNA metabolism (Chen and Shyu, 2011). Previous reports of high-throughput sequencing of RNA isolated through crosslinking immunoprecipitation (HITS-CLIP) have shown that a subpopulation of FUS binds the 3'UTR (Lagier-Tourenne et al., 2012; Ishigaki et al., 2012; Nakaya et al., 2013) and is important for mRNA stability (Kapeli et

al., 2016; Udagawa et al., 2015) and polyadenylation (Masuda et al., 2015), thus suggesting that FUS maintains the expression level of specific mRNAs via control of mRNA stability. However, the mechanism underlying the regulation of mRNA stability by FUS and whether these functions are related to the pathogenesis of FTL/ALS remain unclear.

Synaptic dysfunction has been implicated in a wide range of neurodegenerative diseases, including FTL/ALS (Sephton et al., 2015; Herms and Dorostkar, 2016), and several reports have suggested that it may be an initial process involved in pathological changes (Selkoe, 2002; Jürgens et al., 2016). Previous studies have indicated roles of FUS in synaptic function (Fujii et al., 2005; Qiu et al., 2014; Sephton et al., 2014). In FUS knockdown mice, synaptic dysfunction results in behavioral abnormalities, including hyperactivity and disinhibition (Udagawa et al., 2015, Kino et al., 2015, Ishigaki et al., 2017). In addition, we have shown that FUS regulates GluA1 mRNA stability at the 3'UTR and that GluA1 expression in FUS knockdown mice partially ameliorates these abnormal behaviors (Udagawa et al., 2015). However, it remains unclear how FUS regulates mRNA stability at the 3'UTR and whether GluA1 is the sole major factor responsible for the synaptic abnormalities caused by FUS depletion.

In this study, we identified a major target of FUS, SynGAP spliced isoform $\alpha 2$,

which is a critical factor involved in spine maturation. We found that FUS and ELAV-like proteins cooperatively control SynGAP mRNA stability in a 3'UTR length-dependent manner. Finally, we demonstrated that this mechanism is responsible for the development of abnormal spine morphology and FTL-like cognitive symptoms in FUS knockout mice.

Results

FUS knockdown causes spine abnormalities associated with PSD-95 displacement

To elucidate the mechanisms underlying the dendritic spine abnormalities caused by FUS depletion, we re-evaluated spine morphology in primary hippocampal neurons. F-actin staining by fluorescein-conjugated phalloidin demonstrated a decrease in total spine number, as well as a decrease in the frequency of mature spines in shFUS-induced neurons (Figures 1A-1C), as reported previously (Fujii et al., 2005). This result was consistent with our previous findings showing that FUS depletion in cultured neurons or in the mouse hippocampus decreases synaptic transmission (Udagawa et al., 2015). For further analysis of post-synaptic structure and function, we examined PSD-95 immunocytochemistry. PSD-95 is a major component of the post-synaptic density (PSD). PSD-95 particles were detected in the dendritic spines outside of the dendritic shafts in

control neurons, whereas in FUS-knockdown neurons, the majority of PSD-95 particles were displaced to the inner area of the dendritic shafts (Figures 1D and 1E). However, we found that the protein expression level of PSD-95 remained unchanged according to the results of immunostaining (Figure 1F) and western blotting (Figures 1G and 1H). These data suggest that FUS depletion might affect the protein interaction network of post-synaptic factors and/or cytoskeletal proteins (Halpain et al., 1998).

FUS knockdown downregulates SynGAP expression

To identify proteins whose interaction with PSD-95 is affected in FUS-knockdown neurons, we extracted proteins from cultured neurons and used an anti-PSD-95 antibody in an immunoprecipitation assay (Figure 2A). Liquid chromatography and mass spectrometry (LC/MS) analysis of the bound proteins identified 366 proteins, approximately 12% of which were considered “synapse” proteins according to gene ontology analysis (Figure S1). Eleven of these proteins showed a >2-fold change in the shFUS/shCtrl ratio (Table S1). Here, we focused on SynGAP, which showed a >10-fold lower score for the shFUS/shCtrl ratio, on the basis of the assumption that proteins exhibiting a decreased interaction with PSD-95 would be crucial for spine maturation. Validation of the LC/MS analysis showed that the amount of SynGAP co-

immunoprecipitated with PSD-95 indeed decreased in shFUS neurons (Figures 2B and 2C). However, the input level of SynGAP decreased to a similar extent, indicating that FUS regulates SynGAP expression. Both SynGAP protein (Figures 2D and 2E) and mRNA levels (Figure 2F) were decreased significantly in the FUS knockdown neurons. These data suggest that SynGAP may be a direct target of FUS and that the downregulation of SynGAP may affect spine morphology.

A decrease in SynGAP α 2 is directly involved in abnormal spine maturation in FUS knockdown neurons

SynGAP localizes to the PSD and negatively regulates the Ras/Rap pathway (Kim et al., 1998; Carlisle et al., 2008; Jeyabalan and Clement, 2016), and this protein is associated with autism spectrum disorders and epilepsy (Mignot et al., 2016). Previous studies in SynGAP hetero-knockout mice have identified an increase in the number of mature spines (Kim et al., 2003; Clement et al., 2012; Wang et al., 2013). These results appear contrary to our data. However, SynGAP has been reported to exhibit various alternatively spliced isoforms, and C-terminal variants have opposing effects on synaptic function. For example, overexpression of SynGAP α 1 decreases mEPSC amplitude, whereas SynGAP α 2 increases mEPSC amplitude (McMahon et al., 2012). The sequences

of SynGAP $\alpha 1$ and $\alpha 2$ are thought to be determined by exon 19. The inclusion of exon 19 in the $\alpha 1$ isoform results in a frameshift in exon 20 and a protein product that is shorter than $\alpha 2$. Notably, these previous studies have analyzed the SynGAP $\alpha 1$ isoform. Thus, we consider the possibility that isoform-related control of SynGAP may be associated with synaptic dysfunction in FUS knockdown neurons.

Western blotting and immunostaining analyses of primary hippocampal neurons using isoform-specific antibodies (Figure 3A) showed that only SynGAP $\alpha 2$ was decreased after FUS depletion, whereas the level of SynGAP $\alpha 1$ remained unchanged (Figures 3B-3E), indicating that FUS differentially regulates the expression of SynGAP isoforms. To examine whether SynGAP $\alpha 2$ is a major downstream target of FUS that is involved in spine abnormalities, we generated a SynGAP $\alpha 2$ expression construct (Figures S2A and S2B). The expression of SynGAP $\alpha 2$ rescued the abnormal spine morphology in FUS knockdown neurons (Figures 3F and 3G). However, SynGAP $\alpha 1$ supplementation did not rescue the spine abnormalities observed in FUS-silenced neurons, and SynGAP $\alpha 1$ expression in the control neurons instead enhanced spine abnormalities (Figures 3H and 3I, S2C and S2D), a result consistent with findings from a previous report (McMahon et al., 2012). These data indicated that SynGAP $\alpha 2$ is a major effector of spine maturation that is modulated by FUS.

FUS regulates SynGAP mRNA stability in a 3'UTR length-dependent manner

To elucidate how FUS regulates SynGAP expression, we referred to HITS-CLIP data for FUS from our previous report (Figure S3, Ishigaki et al., 2012). The peak of FUS binding was detected near the 3' end of the SynGAP $\alpha 2$ 3'UTR, a result similar to findings for GluA1 mRNA (Udagawa et al., 2015), thus suggesting that FUS directly binds the SynGAP mRNA 3'UTR and regulates its stability. Indeed, RNA-IP confirmed that FUS bound the SynGAP mRNA (Figure 4A). The mRNA stability assay showed that the mRNA decay rate of the transcripts detected with primers corresponding to the SynGAP mRNA ORF and 3'UTR, but not to the intron, was significantly increased in shFUS neurons compared with shCtrl neurons (Figure 4B).

Because the SynGAP $\alpha 1$ 3'UTR sequence in the Ensembl database appears to be incomplete, we next performed 3'RACE to determine the SynGAP 3'UTR sequence and unexpectedly identified an mRNA variant with a short 3'UTR, in which the internal 3'UTR sequence, including the FUS binding site, appeared to be spliced out. Whereas PCR amplification using a reverse primer designed within the spliced UTR detected a single band, PCR with a reverse primer designed near the 3' end of the 3'UTR resulted in two confirmed bands, corresponding to the full-length (long) and the spliced (short)

3'UTR (Figure 4C). These results indicated that at least two different SynGAP mRNA 3'UTR variants exist: one that is probably modulated by FUS and another that lacks the FUS binding element. The intensity of the short UTR was ~15% compared with the long UTR, and only the mRNA with the long UTR showed a decreased level of FUS knockdown neurons, suggesting that FUS regulates the stability of the long 3'UTR. As the mRNA with the short UTR was not affected by FUS depletion, it is unlikely that alternative splicing of this 3'UTR is affected by FUS depletion (Figures 4D and 4E). qPCR of SynGAP mRNA with the primer pairs specific for SynGAP long3'UTR showed that the SynGAP mRNA level was reduced after FUS knockdown to a similar extent as measured by the primer pairs for the SynGAP ORF (Figures 2F and 4F), suggesting that isoforms with the long 3'UTR are dominant.

Next, to determine which SynGAP isoforms contained the long and the short 3'UTRs, we cloned and sequenced SynGAP mRNA using two sets of primer pairs: one detecting both the short and the long 3'UTRs and another detecting only the long 3'UTR. Interestingly, whereas both SynGAP $\alpha 2$ and $\alpha 1$ were detected by the common primer pair, $\alpha 2$ was the dominant isoform detected by the long UTR-specific primers (Figure 4G). These data suggested that FUS regulates SynGAP mRNAs by binding the specific 3'UTR region in an isoform-dominant manner. Note that the SynGAP $\alpha 1$ sequence available in

the Ensembl database was not found in our sequencing data. However, there was a population of clones in which 1 base in exon 20 was deleted, as compared with the SynGAP $\alpha 2$ sequence, and those clones appeared to be $\alpha 1$ isoforms according to the encoded protein sequence. Because there was only a single base difference in the coding region of the $\alpha 1$ and $\alpha 2$ isoform sequences, we were not able to generate an $\alpha 1$ -specific primer pair to quantify the mRNA level of the $\alpha 1$ isoform specifically. Although SynGAP $\alpha 1$ with the long 3'UTR occurred in some amount, the protein expression level of SynGAP $\alpha 1$ was not decreased by shFUS, and SynGAP $\alpha 1$ supplementation in shFUS neurons did not rescue the spine abnormalities, thus indicating that FUS regulation of SynGAP $\alpha 1$ with a long 3'UTR might have less of an effect on spine morphology.

Finally, to confirm this model, we generated an shRNA targeting the SynGAP 3'UTR, specific to the long UTR containing the FUS binding site (Figure S3). Remarkably, the protein expression of SynGAP $\alpha 2$, but not $\alpha 1$, was decreased in shSynGAP 3'UTR neurons (Figures 4H and 4I), and knockdown by shSynGAP 3'UTR induced spine abnormalities, as observed in FUS-silenced neurons (Figures 4J and 4K). Together, these results strongly suggested that FUS binds a specific region of the SynGAP mRNA 3'UTR and regulates its stability, thus controlling specific isoform expression in a 3'UTR length-dependent manner.

FUS and ELAV-like family proteins regulate SynGAP mRNA stability bidirectionally at its 3'UTR

Next, to further elucidate the precise mechanism underlying the FUS-mediated control of mRNA stability at the 3'UTR, we generated a biotinylated RNA probe for the SynGAP 3'UTR that contained FUS binding sequences (Figure 5A; Figure S3). An RNA pull-down assay using the biotinylated SynGAP 3'UTR and streptavidin beads showed that FUS bound to SynGAP 3'UTR sequences more efficiently than to a control GAPDH probe (Figure S4A). Next, we performed LC/MS analysis of the SynGAP 3'UTR-bound proteins. On the basis of the analysis of in-gel-trypsinized samples from the bands that appeared only when the SynGAP 3'UTR was used as the pull-down probe, we identified many proteins involved in RNA metabolism (Figure S4B, Table S2). Interestingly, we detected several RNA-binding proteins that have been reported to stabilize their target mRNAs (Figures 5B and 5C). We found that the binding efficacy of one of these proteins, ELAV-like protein 4 (ELAVL4/HuD) was significantly decreased in FUS knockdown neurons. We also validated ELAVL3, ELAVL2, PTBP2 and PCBP2, which remained unchanged in pull-down assay (data not shown). Furthermore, we explored proteins that destabilize mRNA (Bronicki et al., 2013) and found that ELAV-like protein 1

(ELAVL1/HuR) bound the SynGAP pull-down probe more strongly in shFUS neurons (Figures 5B and 5C). We also evaluated other RNA-binding proteins that destabilize mRNA, including KSRP, AUF1, CUGBP1 and TIS11B, but no increase in the efficacy of binding to the SynGAP probe was observed (data not shown).

ELAVL4 is an AU-rich element (ARE)-binding protein that regulates mRNA stability (Bronicki et al., 2013; Fukao et al., 2009). FUS co-immunoprecipitation showed that ELAVL4 interacts with FUS independently of RNase (Figure S4C), a result consistent with findings from previous reports (Blokhuys et al., 2016; Groen et al., 2013). More importantly, ELAVL4 knockdown decreased SynGAP α 2 specifically, similarly to FUS knockdown (Figures 5D and 5E). ELAVL4 knockdown also destabilized SynGAP mRNA (Figure 5F). Furthermore, when ELAVL4 was depleted, FUS was released from the SynGAP 3'UTR, and the interaction of ELAVL1 with the SynGAP 3'UTR was increased (Figures 5G and 5H), thus suggesting that FUS and ELAVL proteins cooperatively interact with the SynGAP mRNA 3'UTR and regulate its stability. In support of this notion, double knockdown of FUS and ELAVL4 had no synergistic effect on SynGAP mRNA expression (Figure 5I). On the other hand, individual knockdown of FUS and ELAVL4 both resulted in recruitment of ELAVL1 to the SynGAP pull-down probe (Figures 5B and 5G). ELAVL1 has been reported to stabilize its target mRNAs in

general; however, it has also been found to destabilize certain mRNAs, such as c-Myc mRNA (Mukherjee et al., 2011; Kim et al., 2009). ELAVL1 knockdown increased SynGAP mRNA expression significantly, albeit weakly (Figure 5J), in contrast to the FUS and ELAVL4 knockdown, thus suggesting that ELAVL1 negatively regulates SynGAP mRNA stability. Moreover, ELAVL1 knockdown partially ameliorated SynGAP mRNA expression in shFUS neurons (Figure S4D). To further confirm the regulation of FUS and ELAVL proteins at the SynGAP 3'UTR, we performed a reporter assay using mRNA encoding Venus fluorescent protein fused with a SynGAP 3'UTR sequence identical to the one used in the RNA pulldown assays. Knockdown of FUS, ELAVL4 or ELAVL1 altered reporter expression in the same direction observed for endogenous SynGAP expression in primary cultures (Figures S4E and S4F). Together, these findings indicated that FUS and ELAVL1/4 cooperatively control the stability of SynGAP mRNA at its 3'UTR. This regulation mechanism may also play a role in the control of GluA1 mRNA expression (Figures S4G-S4J), thus suggesting that the FUS-ELAVL protein complex is a common regulator of mRNA stability at the 3'UTR.

Conditional FUS knockout mice show spine abnormalities and FTL/ALS-like behavioral abnormalities, which are ameliorated by SynGAP $\alpha 2$ expression

Finally, to confirm the functional importance of FUS in the control of SynGAP $\alpha 2$ expression, we generated conditional FUS knockout mice in the C57BL/6 strain. The insertion of a LoxP-Cre sequence in FUS and Cre expression controlled by the Camk2-promoter resulted in forebrain-specific knockdown. Immunohistochemistry indicated that the FUS expression level was decreased in the hippocampus (Figure 6A). Lysates from the CA1 region of the hippocampus exhibited decreased expression of SynGAP $\alpha 2$, but not $\alpha 1$, a result similar to that in primary neurons (Figures 6B and 6C). Fluorescence immunohistochemistry of CA1 also revealed a decrease in SynGAP $\alpha 2$ expression (Figure 6D). Golgi-Cox staining showed that the proportion of mature dendritic spines was significantly decreased in CA1 dendrites, but the number of spines remained unchanged (Figures 6E-6G). This phenotype was similar to that of adeno-associated virus (AAV)-shFUS injected mice (Udagawa et al., 2015, Ishigaki et al., 2017) and was ameliorated by SynGAP $\alpha 2$ expression via AAV (Figures 6E-6G; Figures S5A and S5B). These data indicated that SynGAP $\alpha 2$ is an important modulator of spine maturation *in vivo* in the FUS knockdown model.

Behavioral assays revealed that conditional FUS knockout mice showed hyperactivity in an open-field test (OFT) (Figure 6H) and decreased anxiety in an elevated plus-maze test (EPM) (Figures 6I and 6J). However, memory defects were absent in the

novel object recognition test (NOR) (Figure S5C) and the fear conditioning test (FC) (Figures S5E and S5F). These phenotypes were similar to those of previous FUS knockdown models (Udagawa et al., 2015; Kino et al., 2015), suggesting the existence of common features in FUS depletion models. Moreover, the phenotype of disinhibition in the absence of a memory defect partially mimics the early symptoms of FTLD (Vernay et al., 2016; Rascovsky et al., 2011). Whereas AAV-shFUS-injected mice showed increased interactions in the social interaction test (SI) and an increase in object investigation in the NOR (Udagawa et al., 2015), conditional FUS knockout mice did not show these phenotypes (Figures S5D and S5G). Finally, to confirm that the decrease in SynGAP $\alpha 2$ levels was responsible for these behavioral abnormalities, we injected AAV-SynGAP $\alpha 2$ into the FUS knockout mice. SynGAP $\alpha 2$ supplementation in the hippocampus indeed partially ameliorated the observed phenotypes (Figures 6H-6J). Supplementation of SynGAP $\alpha 2$ in wild-type mice had no effect on their behavior in these assays (Figures S5H-S5J). These results, together with those from our previous work, suggested that the cognitive and synaptic disabilities induced by the loss of FUS function can be ameliorated by enhancing synaptic function through the induction of spine maturation or synaptic glutamate receptors. This result may provide an effective strategy for the prevention of neurodegenerative disease progression.

Discussion

RNA-binding proteins related to FTLD/ALS, such as FUS and TDP-43, have been implicated in RNA metabolism; however, the underlying mechanisms directly linked to physiology or pathogenesis remain unclear. We found that SynGAP $\alpha 2$ is a major target of FUS in the promotion of spine maturation and cognitive function in 3'UTR length-dependent manner. These results, together with our previous finding that GluA1 expression is regulated by FUS (Udagawa et al., 2015), notably suggest that the expression of two functionally distinct proteins at the post-synapse, SynGAP $\alpha 2$ and GluA1, an AMPA receptor subunit, are both capable of rescuing the spine abnormalities and cognitive function deficits caused by FUS depletion. The pathogenesis of FTLD/ALS has been mainly described in the context of the gain of toxic function model (Ling et al., 2013). Our loss of function model displayed spine abnormality, which is thought to be an initial change in neurodegeneration (Selkoe, 2002; Herms and Dorostkar, 2016), as well as a few selected behavioral abnormalities, partially reminiscent of FTLD symptoms. These data suggest that FUS deficiency might also be involved in the disease mechanism of FTLD/ALS. Certainly, further evaluation in other brain regions and human samples will be needed to clarify whether these abnormalities caused by FUS depletion indeed

contribute to FTLD/ALS pathogenesis.

Because the 3'UTR plays a role in controlling mRNA stability, localization, and translation, an alternative 3'UTR may significantly affect the destination of the corresponding mRNAs (Tian and Manley, 2017; Mayr, 2016). We found that SynGAP isoforms exhibit at least two different forms of the 3'UTR: full length (long) and alternately spliced (short). We showed that FUS controls the expression of the $\alpha 2$ isoform, but not the $\alpha 1$ isoform and that SynGAP $\alpha 2$ is the major isoform that possesses the long 3'UTR, in which the FUS binding site is present. Such 3'UTR length-dependent regulation of mRNA stability has been reported previously (Graham et al., 2007; Sandberg et al., 2008), but not for RNA-binding proteins related to FTLD/ALS. Although the precise mechanism of SynGAP 3'UTR splicing remains unknown, it would be interesting to elucidate the different functions of each alternative 3'UTR that may be involved in spine morphology or localized to a certain subcellular region (An et al., 2008; Berkovits and Mayr, 2015).

We found that SyGAP $\alpha 2$ is the major isoform with long 3'UTR, whereas majority of the $\alpha 1$ isoform have short 3'UTR and SynGAP β exhibits both short and long 3'UTR. SynGAP $\alpha 1$ has been the most characterized SynGAP isoform thus far, and is reported to interact with PSD-95 through its C-terminal PDZ ligand motif (Kim et al.,

1998). The deletion of the PDZ ligand motif has been shown to disrupt its interaction with PSD-95, resulting in enlarged spines (Vazquez et al., 2004). The phosphorylation of SynGAP α 1 by CaMKII and PLK2 modulates the composition of the PSD by reducing its occupancy of the PDZ domain of PSD-95, which, in turn, would free the PDZ domain for binding with other proteins (Walkup et al., 2016). Although neither SynGAP α 2 nor SynGAP β have a PDZ ligand motif, they have been shown to localize to PSD (McMahon et al., 2012). As SynGAP might form trimers through its coiled-coil domains (Zeng et al., 2016), SynGAP α 2, and possibly β , might indirectly interact with PSD-95. As precise interaction or localization of SynGAP isoforms remain unclear, further evaluation will be needed to elucidate the functions of each isoform, the cooperative effects of the isoforms, and the involvement of 3'UTR length-dependent regulation.

We showed that FUS binds ELAVL4 at a unique position within the SynGAP long 3'UTR. ELAVL4 has various roles in RNA metabolism, including functions related to alternative splicing, translation, alternative polyadenylation, mRNA transport, and mRNA stability (Bronicki et al., 2013; Fukao et al., 2009). ELAVL4 KO mice show deficits in dendritogenesis and a lack of anxiety in an EPM, similarly to our FUS knockout mice (DeBoer et al., 2014). However, the involvement of ELAVL4 in FTL/ALS has not been adequately investigated (Fallini et al., 2012). We demonstrated that depletion of

either FUS or ELAVL4 accelerated the decay of SynGAP $\alpha 2$ mRNA. Interestingly, knockdown of one of these proteins decreased the SynGAP 3'UTR-binding efficacy of the other, and double knockdown of FUS and ELAVL4 did not have a synergistic effect on SynGAP mRNA expression, thus suggesting that FUS and ELAVL4 act together in stabilizing SynGAP mRNA. Moreover, we demonstrated that ELAVL1, the counterpart of the FUS-ELAVL4 complex, destabilizes SynGAP mRNA. Knockdown of ELAVL1 partially ameliorated the decrease in SynGAP mRNA due to FUS depletion. ARE-binding proteins (ARE-BPs), including ELAVL proteins, regulate ARE-BP-mediated decay (Chen and Shyu, 2011) and collaborate or act antagonistically at ARE-containing 3'UTRs, thereby balancing target mRNA expression (Iadevaia and Gerber, 2015; Gardiner et al., 2015). The counterpart of ELAVL4 for ARE-mediated decay has been suggested (Gardiner et al., 2015), but not verified. Interestingly, GluA1 expression is regulated in a similar manner as SynGAP by ELAVL4 and ELAVL1, thus suggesting that cooperative control of mRNA stability by FUS and ELVAL proteins might be a conserved mechanism for the regulation of synaptic proteins. However, because the rescue efficacy of shELAVL1 was limited, other factors, such as miRNAs, may be involved in ELAVL1-mediated SynGAP mRNA destabilization (Kim et al., 2009; Glorian et al., 2011). Future studies will be needed to determine how the mRNA stabilization and decay of SynGAP

mRNA are balanced and whether/how this mechanism is disrupted under certain circumstances that cause neurodegenerative diseases, including environmental stress or aging.

In summary, we identified SynGAP $\alpha 2$ as a major candidate target that is involved in spine maturation and cognitive behavior and is regulated by FUS. In addition, we demonstrated that FUS, together with ELAVL family proteins, regulates SynGAP mRNA stability at a unique sequence within the long 3'UTR, thus stabilizing the long UTR-specific mRNA. Our findings increase our understanding of the pathways controlled by FUS function and provide important clues for the further exploration of the pathogenesis of FTL/D/ALS.

Experimental Procedures

Animals

All mice (C57BL/6J) were maintained in a temperature (25 °C) and light-controlled (12 h light-dark cycle) facility. Animal protocols were approved by the Institutional Committee under the Regulations for Animal Experiments at Nagoya University. We generated conditional FUS knockout mice by using the loxP-Cre system. The same directional loxP sites were inserted into the 5'UTR and intron 3 of the FUS gene with a Frt-flanked neomycin cassette. Targeted iTL BA1 (C57BL/6J x 129/SvEv) hybrid embryonic stem cells were microinjected into C57BL/6J blastocysts. The resulting chimeras were mated with C57BL/6J FLP mice to remove the Neo cassette and were backcrossed to C57BL/6J. MAX-BAXSM (Charles River) was performed to obtain fully congenic mice for behavioral assays. Finally, we crossed FUS flox/flox mice with Camk2-Cre mice (Tsien et al., 1996, a kind gift from Miyakawa T) and generated FUS^{fl/fl} Cre+ mice as conditional FUS knockout mice and FUS^{fl/fl} or FUS^{fl/-} Cre- mice, which were used as controls.

Neuron cultures

Cultures of mouse cortical and hippocampal neurons were prepared as described

previously (Udagawa et al., 2015). Details regarding neuron culture, western blotting, immunostaining, immunoprecipitation, quantitative real-time PCR, RNA pull-down assays, reporter assays, DNA construction, Lentivirus production, and AAV production are presented in the Supplemental Experimental Procedures.

Quantitative analysis of immunofluorescence data and spine morphology

The immunofluorescence signal intensity was measured using ZEN software (Zeiss). The nucleus was determined based on the DAPI-positive area, and the cell body cytoplasm was determined based on the MAP2-positive/DAPI-negative area. The ROI of the soma was set to equally include areas of the nucleus and the cytoplasm, blinded from interested protein intensities. The dendrite intensity measurement and counts of PSD-95 particles were performed using ImageJ software. The equal ROI area, 20 μm in length and 5 μm in width within the range of 40-100 μm away from the cell soma without other crossed dendrites, was set to measure the mean intensity of PSD-95, including the inside and outside of the dendrites. Note that no more than one 20- μm section per dendritic branch within this range can be selected in most cases, which is due to high confluency of crossed dendrites. Particles inside and outside the MAP2-positive area were counted by using the “particle count” function in ImageJ. The threshold was set to twice the mean intensity for

the shCtrl dendrites. The number of spines was counted over a region of 10 μm in length, selected by applying the same criterion as above. In the same region, mature spines were analyzed on the basis of the definition of a head/neck diameter ratio >1.5 (Harris et al., 1992). In all experiments, MAP2 intensities were analyzed, and no significant differences were found between groups.

Behavioral assays

Behavioral assays were conducted on the male mice at 12-15 weeks of age. Mice were examined using the open field test, elevated plus maze test, novel object recognition test, social interaction test, and fear conditioning test under the same experimental settings, as described previously (Udagawa et al., 2015). The mice were used for each behavioral test only once. The precise settings for each assay are described in the Supplemental Experimental Procedures.

Statistical analyses

Western blot, immunocytochemistry, immunoprecipitation, and qRT-PCR data were obtained from at least three independent experiments. All data were analyzed with IBM SPSS Statics 24. Normality was determined with the Shapiro-Wilk test. For the statistical

analysis of two groups, the unpaired t-test was used (except in Figure S6C, where the data were analyzed with a paired t-test). When the data were not distributed normally, the Mann-Whitney U-test was used. In experiments with more than two groups, one-way analysis of variance with post hoc Tukey's multiple comparison test was used. When the data were not normally distributed, the Kruskal-Wallis test and the post hoc Bonferroni test were used. In the mRNA stability assay presented in Figures 4B and 5F, ANCOVA was used for the analysis of fitted curves. In all experiments, the data are expressed as the mean \pm s.e.m., and the threshold of statistical significance was set to *P<0.05, **P<0.01, or ***P<0.001.

Author contributions

Conceptualization, S.Y., T.U., S.I. and G.S.; Methodology, S.Y., T.U. and S.I.; Investigation, S.Y., D.H., Y.F., S.I. and T.U.; Resources, S.I. and H.O.; Formal Analysis, S.Y.; Visualization, S.Y., T.U., S.I., and G.S.; Writing-Original Draft, S.Y. and T.U.; Writing-Review & Editing, S.I., H.W., M.K., and G.S.; Funding Acquisition, G.S.; Supervision, G.S.

Accession numbers

The full LC/MS data reported in this study were deposited in ProteomeXchange and jPOST. The accession numbers for the PSD-95 Co-IP experiment are PXD007522 and JPST000302. The accession numbers for the RNA-pull down assay are PXD007521 and JPST000303.

Acknowledgements

We thank P.C. Kind for the kind gift of plasmids, Tsuyoshi Miyakawa for the kind gift of Camk2-Cre mice, Akiko Miwa and Sayaka Hirai for technical support in AAV production, Natalie G. Farny for critical reading of the manuscript and Kentaro Taki for operational support in LC/MS/MS in the laboratory of the Division for Medical Research Engineering, Nagoya University Graduate School of Medicine. A part of this study represents the results of the “Integrated Research on Neuropsychiatric Disorders” and “Integrated Research on Depression, Dementia and Development Disorders” projects carried out under the Strategic Research Program for Brain Sciences and Brain/MINDS of the Ministry of Education, Culture, Sports, Science and Technology of Japan and the Japan Agency for Medical Research and Development. This work was also supported by a Mext Grant-in-aid project, Scientific Research on Innovation Area (Brain Protein Aging and Dementia control).

References

An, J.J., Gharami, K., Liao, G.Y., Woo, N.H., Lau, A.G., Vanevski, F., Torre, E.R., Jones, K.R., Feng, Y., Lu, B., et al. (2008). Distinct role of long 3' UTR BDNF mRNA in spine morphology and synaptic plasticity in hippocampal neurons. *Cell* 134, 175-187.

Berkovits, B.D., and Mayr, C. (2015). Alternative 3' UTRs act as scaffolds to regulate membrane protein localization. *Nature* 522, 363-367.

Blokhuys, A.M., Koppers, M., Groen, E.J., van den Heuvel, D.M., Dini Modigliani, S., Anink, J.J., Fumoto, K., van Diggelen, F., Snelting, A., Sooda, P., et al. (2016). Comparative interactomics analysis of different ALS-associated proteins identifies converging molecular pathways. *Acta Neuropathol* 132, 175-196.

Bronicki, L.M., and Jasmin, B.J. (2013). Emerging complexity of the HuD/ELAV14 gene; implications for neuronal development, function, and dysfunction. *RNA* 19, 1019-1037.

Carlisle, H.J., Manzerra, P., Marcora, E., and Kennedy, M.B. (2008). SynGAP regulates steady-state and activity-dependent phosphorylation of cofilin. *J Neurosci* 28, 13673-

13683.

Chen, C.Y., and Shyu, A.B. (2011). Mechanisms of deadenylation-dependent decay. *Wiley Interdiscip. Rev. RNA* 2, 167-183.

Clement, J.P., Aceti, M., Creson, T.K., Ozkan, E.D., Shi, Y., Reish, N.J., Almonte, A.G., Miller, B.H., Wiltgen, B.J., Miller, C.A., et al. (2012). Pathogenic SYNGAP1 mutations impair cognitive development by disrupting maturation of dendritic spine synapses. *Cell* 151, 709-723.

DeBoer, E.M., Azevedo, R., Vega, T.A., Brodtkin, J., Akamatsu, W., Okano, H., Wagner, G.C., and Rasin, M.R. (2014). Prenatal deletion of the RNA-binding protein HuD disrupts postnatal cortical circuit maturation and behavior. *J. Neurosci.* 34, 3674-3686.

Fallini, C., Bassell, G.J., and Rossoll, W. (2012). The ALS disease protein TDP-43 is actively transported in motor neuron axons and regulates axon outgrowth. *Hum. Mol. Genet.* 21, 3703-3718.

Fujii, R., Okabe, S., Urushido, T., Inoue, K., Yoshimura, A., Tachibana, T., Nishikawa, T., Hicks, G.G., and Takumi, T. (2005). The RNA binding protein TLS is translocated to dendritic spines by mGluR5 activation and regulates spine morphology. *Curr. Biol.* 15, 587-593.

Fukao, A., Sasano, Y., Imataka, H., Inoue, K., Sakamoto, H., Sonenberg, N., Thoma, C., and Fujiwara, T. (2009). The ELAV protein HuD stimulates cap-dependent translation in a Poly(A)- and eIF4A-dependent manner. *Mol. Cell* 36, 1007-1017.

Gardiner, A.S., Twiss, J.L., and Perrone-Bizzozero, N.I. (2015). Competing Interactions of RNA-Binding Proteins, MicroRNAs, and Their Targets Control Neuronal Development and Function. *Biomolecules* 5, 2903-2918.

Glorian, V., Maillot, G., Poles, S., Iacovoni, J.S., Favre, G., and Vagner, S. (2011). HuR-dependent loading of miRNA RISC to the mRNA encoding the Ras-related small GTPase RhoB controls its translation during UV-induced apoptosis. *Cell Death Differ.* 18, 1692-1701.

Graham, R.R., Kyogoku, C., Sigurdsson, S., Vlasova, I.A., Davies, L.R., Baechler, E.C., Plenge, R.M., Koeuth, T., Ortmann, W.A., Hom, G., et al. (2007). Three functional variants of IFN regulatory factor 5 (IRF5) define risk and protective haplotypes for human lupus. *Proc Natl Acad Sci U S A* 104, 6758-6763.

Groen, E.J., Fumoto, K., Blokhuis, A.M., Engelen-Lee, J., Zhou, Y., van den Heuvel, D.M., Koppers, M., van Diggelen, F., van Heest, J., Demmers, J.A., et al. (2013). ALS-associated mutations in FUS disrupt the axonal distribution and function of SMN. *Hum. Mol. Genet.* 22, 3690-3704.

Halpain, S., Hipolito, A., and Saffer, L. (1998). Regulation of F-actin stability in dendritic spines by glutamate receptors and calcineurin. *J Neurosci* 18, 9835-9844.

Harris, K.M., Jensen, F.E., and Tsao, B. (1992). 3-Dimensional Structure of Dendritic Spines and Synapses in Rat Hippocampus (Ca1) at Postnatal Day-15 and Adult Ages - Implications for the Maturation of Synaptic Physiology and Long-Term Potentiation. *J. Neurosci.* 12, 2685-2705.

Herns, J., and Dorostkar, M.M. (2016). Dendritic Spine Pathology in Neurodegenerative Diseases. *Annu. Rev. Pathol.* 11, 221-250.

Iadevaia, V., and Gerber, A.P. (2015). Combinatorial Control of mRNA Fates by RNA-Binding Proteins and Non-Coding RNAs. *Biomolecules* 5, 2207-2222.

Ishigaki, S., Masuda, A., Fujioka, Y., Iguchi, Y., Katsuno, M., Shibata, A., Urano, F., Sobue, G., and Ohno, K. (2012). Position-dependent FUS-RNA interactions regulate alternative splicing events and transcriptions. *Sci Rep* 2, 529.

Ishigaki, S., Fujioka, Y., Okada, Y., Riku, Y., Udagawa, T., Honda, D., Yokoi, S., Endo, K., Ikenaka, K., Takagi, S., et al. (2017). Altered Tau Isoform Ratio Caused by Loss of FUS and SFPQ Function Leads to FTL-like Phenotypes. *Cell Rep.* 18, 1118-1131.

Jeyabalan, N., and Clement, J.P. (2016). SYNGAP1: Mind the Gap. *Front. Cell. Neurosci* 10, 32.

Jürgens, T., Jafari, M., Kreutzfeldt, M., Bahn, E., Bruck, W., Kerschensteiner, M., and

Merkler, D. (2016). Reconstruction of single cortical projection neurons reveals primary spine loss in multiple sclerosis. *Brain* 139, 39-46.

Kapeli, K., Pratt, G.A., Vu, A.Q., Hutt, K.R., Martinez, F.J., Sundararaman, B., Batra, R., Freese, P., Lambert, N.J., Huelga, S.C., et al. (2016). Distinct and shared functions of ALS-associated proteins TDP-43, FUS and TAF15 revealed by multisystem analyses. *Nat Commun* 7, 12143.

Kim, H.H., Kuwano, Y., Srikantan, S., Lee, E.K., Martindale, J.L., and Gorospe, M. (2009). HuR recruits let-7/RISC to repress c-Myc expression. *Genes Dev.* 23, 1743-1748.

Kim, J.H., Lee, H.K., Takamiya, K., and Huganir, R.L. (2003). The role of synaptic GTPase-activating protein in neuronal development and synaptic plasticity. *J. Neurosci.* 23, 1119-1124.

Kim, J.H., Liao, D., Lau, L.F., and Huganir, R.L. (1998). SynGAP: a synaptic RasGAP that associates with the PSD-95/SAP90 protein family. *Neuron* 20, 683-691.

Kino, Y., Washizu, C., Kurosawa, M., Yamada, M., Miyazaki, H., Akagi, T., Hashikawa, T., Doi, H., Takumi, T., Hicks, G.G., et al. (2015). FUS/TLS deficiency causes behavioral and pathological abnormalities distinct from amyotrophic lateral sclerosis. *Acta Neuropathol. Commun.* 3, 24.

Kwiatkowski, T.J., Bosco, D.A., LeClerc, A.L., Tamrazian, E., Vanderburg, C.R., Russ, C., Davis, A., Gilchrist, J., Kasarskis, E.J., Munsat, T., et al. (2009). Mutations in the FUS/TLS Gene on Chromosome 16 Cause Familial Amyotrophic Lateral Sclerosis. *Science* 323, 1205-1208.

Lagier-Tourenne, C., Polymenidou, M., Hutt, K.R., Vu, A.Q., Baughn, M., Huelga, S.C., Clutario, K.M., Ling, S.C., Liang, T.Y., Mazur, C., et al. (2012). Divergent roles of ALS-linked proteins FUS/TLS and TDP-43 intersect in processing long pre-mRNAs. *Nat Neurosci* 15, 1488-1497.

Ling, S.C., Polymenidou, M., and Cleveland, D.W. (2013). Converging mechanisms in ALS and FTD: disrupted RNA and protein homeostasis. *Neuron* 79, 416-438.

Mackenzie, I.R., Ansorge, O., Strong, M., Bilbao, J., Zinman, L., Ang, L.C., Baker, M., Stewart, H., Eisen, A., Rademakers, R., et al. (2011). Pathological heterogeneity in amyotrophic lateral sclerosis with FUS mutations: two distinct patterns correlating with disease severity and mutation. *Acta Neuropathol* 122, 87-98.

Masuda, A., Takeda, J.I., Okuno, T., Okamoto, T., Ohkawara, B., Ito, M., Ishigaki, S., Sobue, G., and Ohno, K. (2015). Position-specific binding of FUS to nascent RNA regulates mRNA length. *Genes Dev.* 29, 1045-1057.

Mayr, C. (2016). Evolution and Biological Roles of Alternative 3'UTRs. *Trends Cell Biol* 26, 227-237.

McMahon, A.C., Barnett, M.W., O'Leary, T.S., Stoney, P.N., Collins, M.O., Papadia, S., Choudhary, J.S., Komiyama, N.H., Grant, S.G., Hardingham, G.E., et al. (2012). SynGAP isoforms exert opposing effects on synaptic strength. *Nat Commun* 3, 900.

Mignot, C., von Stulpnagel, C., Nava, C., Ville, D., Sanlaville, D., Lesca, G., Rastetter, A., Gachet, B., Marie, Y., Korenke, G.C., et al. (2016). Genetic and neurodevelopmental

spectrum of SYNGAP1-associated intellectual disability and epilepsy. *J. Med. Genet.* 53, 511-522.

Morlando, M., Dini Modigliani, S., Torrelli, G., Rosa, A., Di Carlo, V., Caffarelli, E., and Bozzoni, I. (2012). FUS stimulates microRNA biogenesis by facilitating co-transcriptional Drosha recruitment. *EMBO J.* 31, 4502-4510.

Mukherjee, N., Corcoran, D.L., Nusbaum, J.D., Reid, D.W., Georgiev, S., Hafner, M., Ascano, M., Jr., Tuschl, T., Ohler, U., and Keene, J.D. (2011). Integrative regulatory mapping indicates that the RNA-binding protein HuR couples pre-mRNA processing and mRNA stability. *Mol. Cell* 43, 327-339.

Nakaya, T., Alexiou, P., Maragkakis, M., Chang, A., and Mourelatos, Z. (2013). FUS regulates genes coding for RNA-binding proteins in neurons by binding to their highly conserved introns. *RNA* 19, 498-509.

Neumann, M., Rademakers, R., Roeber, S., Baker, M., Kretschmar, H.A., and Mackenzie, I.R. (2009). A new subtype of frontotemporal lobar degeneration with FUS

pathology. *Brain* 132, 2922-2931.

Qiu, H., Lee, S., Shang, Y., Wang, W.Y., Au, K.F., Kamiya, S., Barmada, S.J., Finkbeiner, S., Lui, H., Carlton, C.E., et al. (2014). ALS-associated mutation FUS-R521C causes DNA damage and RNA splicing defects. *J. Clin. Invest.* 124, 981-999.

Rascovsky, K., Hodges, J.R., Knopman, D., Mendez, M.F., Kramer, J.H., Neuhaus, J., van Swieten, J.C., Seelaar, H., Dopper, E.G., Onyike, C.U., et al. (2011). Sensitivity of revised diagnostic criteria for the behavioural variant of frontotemporal dementia. *Brain* 134, 2456-2477.

Sandberg, R., Neilson, J.R., Sarma, A., Sharp, P.A., and Burge, C.B. (2008). Proliferating cells express mRNAs with shortened 3' untranslated regions and fewer microRNA target sites. *Science* 320, 1643-1647.

Seelaar, H., Rohrer, J.D., Pijnenburg, Y.A., Fox, N.C., and van Swieten, J.C. (2011). Clinical, genetic and pathological heterogeneity of frontotemporal dementia: a review. *J. Neurol. Neurosurg. Psychiatry* 82, 476-486.

Selkoe, D.J. (2002). Alzheimer's disease is a synaptic failure. *Science* 298, 789-791.

Sephton, C.F., Tang, A.A., Kulkarni, A., West, J., Brooks, M., Stubblefield, J.J., Liu, Y., Zhang, M.Q., Green, C.B., Huber, K.M., et al. (2014). Activity-dependent FUS dysregulation disrupts synaptic homeostasis. *Proc. Natl. Acad. Sci. USA* 111, E4769-4778.

Sephton, C.F., and Yu, G. (2015). The function of RNA-binding proteins at the synapse: implications for neurodegeneration. *Cell. Mol. Life Sci.* 72, 3621-3635.

Tan, A.Y., and Manley, J.L. (2010). TLS Inhibits RNA Polymerase III Transcription. *Mol. Cell. Biol.* 30, 186-196.

Tian, B., and Manley, J.L. (2017). Alternative polyadenylation of mRNA precursors. *Nat Rev Mol Cell Biol* 18, 18-30.

Tsien, J.Z., Chen, D.F., Gerber, D., Tom, C., Mercer, E.H., Anderson, D.J., Mayford, M.,

Kandel, E.R., and Tonegawa, S. (1996). Subregion- and cell type-restricted gene knockout in mouse brain. *Cell* 87, 1317-1326.

Udagawa, T., Fujioka, Y., Tanaka, M., Honda, D., Yokoi, S., Riku, Y., Ibi, D., Nagai, T., Yamada, K., Watanabe, H., et al. (2015). FUS regulates AMPA receptor function and FTL/ALS-associated behaviour via GluA1 mRNA stabilization. *Nat Commun* 6, 7098.

Vazquez, L.E., Chen, H.J., Sokolova, I., Knuesel, I., and Kennedy, M.B. (2004). SynGAP regulates spine formation. *J Neurosci* 24, 8862-8872.

Vernay, A., Sellal, F., and Rene, F. (2016). Evaluating Behavior in Mouse Models of the Behavioral Variant of Frontotemporal Dementia: Which Test for Which Symptom? *Neurodegener. Dis.* 16, 127-139.

Walkup, W.G., Mastro, T.L., Schenker, L.T., Vielmetter, J., Hu, R., Iancu, A., Reghunathan, M., Bannon, B.D., and Kennedy, M.B. (2016). A model for regulation by SynGAP-alpha1 of binding of synaptic proteins to PDZ-domain 'Slots' in the postsynaptic density. *eLife* 5.

Wang, C.C., Held, R.G., and Hall, B.J. (2013). SynGAP regulates protein synthesis and homeostatic synaptic plasticity in developing cortical networks. *Plos One* 8, e83941.

Yasuda, K., Zhang, H., Loisel, D., Haystead, T., Macara, I.G., and Mili, S. (2013). The RNA-binding protein Fus directs translation of localized mRNAs in APC-RNP granules. *J. Cell Biol.* 203, 737-746.

Zeng, M., Shang, Y., Araki, Y., Guo, T., Huganir, R.L., and Zhang, M. (2016). Phase Transition in Postsynaptic Densities Underlies Formation of Synaptic Complexes and Synaptic Plasticity. *Cell* 166, 1163-1175 e1112.

Figure legends**Figure 1. FUS knockdown causes spine abnormalities with PSD-95 displacement in cultured neurons.**

(A) Mouse primary hippocampal neurons were infected with a lentivirus expressing scrambled shRNA (shCtrl) or shRNA targeting FUS (shFUS1 and shFUS2). At DIV20, the neurons were immunostained for FUS (white) and MAP2 (red). F-actin (green) was stained by fluorescein-conjugated phalloidin. Mature spines are indicated with red arrows. Low magnification: Scale bar = 20 μm . High magnification: Scale bar = 5 μm . (B) Quantification of the soma FUS intensity in (A) (n = 19, 18, and 19 neurons from triplicate samples for shCtrl, shFUS1, and shFUS2, respectively; Kruskal-Wallis test; ***P < 0.001 compared with shCtrl). (C) Quantification of the number of spines per 1 μm and the percentage of mature spines in (A) (n = 19, 18, and 19 neurons for shCtrl, shFUS1, and shFUS2; one-way analysis of variance; ***P < 0.001 compared with shCtrl). (D) Immunostaining of primary hippocampal neurons for PSD-95 (green) and MAP2 (red) (n = 21, 17, and 17 neurons from triplicate samples for shCtrl, shFUS1, and shFUS2). High magnification: Scale bar = 5 μm . Low magnification: Scale bar = 20 μm . (E) Quantification of the percentage of PSD-95-positive particles outside of the dendrite in (D) with ImageJ software (one-way analysis of variance; ***P < 0.001 compared with

shCtrl). (F) Quantification of the intensity of soma and dendrite PSD-95 in (D) (NS = not significant, one-way analysis of variance). (G) The lysates of primary hippocampal neurons were subjected to western blotting with the indicated antibodies (n = 3 each). (H) Quantification of the protein levels in (G) (normalized to GAPDH intensity; one-way analysis of variance; **P < 0.01, ***P < 0.001 compared with shCtrl). In (B), (C), (E), (F) and (H), data represent mean \pm SEM.

Figure 2. SynGAP is downregulated in FUS knockdown neurons.

(A) Schematic representation of the mass spectrometry analysis of PSD-95-bound proteins in the control and FUS knockdown primary cortical neurons. (B) Co-IP of PSD-95 using the lysates from the FUS knockdown and control primary cortical neurons (n = 3 each). The bound proteins were detected by western blotting with the indicated antibodies. (C) Quantification of the band intensity of SynGAP in (B) (*P < 0.05, ***P < 0.001, un-paired t-test). (D) The lysates were prepared from primary hippocampal neurons infected with shCtrl, shFUS1 and shFUS2 (n = 4 neuron cultures each) and were subjected to western blotting with the indicated antibodies. (E) Quantification of the band intensity of SynGAP in (D) (normalized to GAPDH intensity; one-way analysis of variance; *P < 0.05, **P < 0.01 compared with shCtrl). (F) Total RNA was extracted

from primary hippocampal neurons infected with shCtrl, shFUS1 and shFUS2 (n = 3 neuron cultures each), and the mRNA expression levels of SynGAP and FUS were analyzed via qRT-PCR (one-way analysis of variance; *P < 0.05, **P < 0.01 compared with shCtrl). In (C), (E) and (F), data represent mean \pm SEM. See also Figure S1.

Figure 3. The decrease in SynGAP α 2 is responsible for spine abnormalities in the FUS knockdown neurons.

(A) Neuro2A cells were transfected with the lentivirus vectors expressing SynGAP α 1 or α 2 with FLAG, and the lysates were analyzed by western blotting with the indicated antibodies. (B) Lysates were prepared from primary hippocampal neurons infected with shCtrl and shFUS1 (shFUS) (n = 3 each) and were subjected to western blotting with the indicated antibodies. (C) Quantification of the band intensity shown in (B) (normalized to GAPDH intensity; *P < 0.05, un-paired t-test). (D) Primary hippocampal neurons infected with shCtrl and shFUS were immunostained for SynGAP α 2 or α 1 (red), FUS (white) and MAP2 (green). Scale bar = 50 μ m. (E) Quantification of SynGAP soma intensity in (D) (**P < 0.01, un-paired t-test). (F) Primary hippocampal neurons infected with shCtrl + mock (n = 22), shFUS + mock (n = 22), shCtrl + SynGAP α 2 (n = 24) or shFUS + SynGAP α 2 (n = 20) were immunostained for MAP2 (red). F-actin (green)

was stained by fluorescein-conjugated phalloidin. Mature spines are indicated with red arrows. Scale bar = 5 μm . (G) Quantification of the number of spines per 1 μm and the percentage of mature spines in (F) (**P < 0.01, one-way analysis of variance). (H) Primary hippocampal neurons infected with shCtrl + mock (n = 20), shFUS + mock (n = 20), shCtrl + SynGAP $\alpha 1$ (n = 22) and shFUS + SynGAP $\alpha 1$ (n = 21) were immunostained for MAP2 (red). F-actin (green) was stained by fluorescein-conjugated phalloidin. Scale bar = 5 μm . (I) Quantification of the number of spines and the percentage of mature spines in (H) (spine number: **P < 0.01, one-way analysis of variance; %mushroom spine: **P < 0.01, Kruskal-Wallis test). In (C), (E), (G) and (I), data represent mean \pm SEM. See also Figure S2.

Figure 4. FUS regulates the stability of SynGAP $\alpha 2$ mRNA at its 3'UTR in a 3'UTR length-dependent manner.

(A) RNA IP of FUS in cultured cortical neurons. The bound RNAs were analyzed via qRT-PCR. IP efficiency was calculated relative to the input. Representative data from triplicate experiments are shown. (B) mRNA stability was measured in the control and FUS knockdown primary cortical neurons treated with 10 $\mu\text{g ml}^{-1}$ actinomycin D via qRT-PCR using the primer sets indicated above each graph. The RNA level relative to

pretreatment samples for an equal amount of total RNA is plotted against the time after treatment (**P < 0.01, ***P < 0.001, ANCOVA). (C) RT-PCR of RNA from primary hippocampal neuron cultures was performed by using the 2 primer sets indicated in the schema. The band corresponding to the short UTR, indicated by a yellow arrow, was extracted, and its sequence is shown beside the gel image. A putative splice junction is indicated with an arrow. (D) RT-PCR of SynGAP 3'UTR in primary hippocampal neurons infected with shCtrl or shFUS were performed with the primer No.2 set as shown in (C) (n = 3 each). (E) The band intensity was quantified by ImageJ software (***P < 0.001, unpaired t- test). (F) SynGAP mRNA levels in primary hippocampal neurons infected with shCtrl or shFUS (n=3 each) were analyzed via qRT-PCR using primers for the long 3'UTR specific sequence (**P < 0.01, un-paired t-test). (G) Two reverse primers, one containing the sequence of the 3' end of the 3'UTR and the other 400 nt from exon 20, were designed to detect the ratio of SynGAP isoforms in primary hippocampal neurons (n=56 for R primer1, n=50 for R primer2). (H) Lysates from primary cortical neurons infected with shCtrl or shSynGAP 3'UTR (n = 3 each) were analyzed by western blotting with the indicated antibodies. (I) Quantification of the protein levels in (H) (normalized to GAPDH intensity; *P < 0.05, un-paired t-test). (J) Primary hippocampal neurons infected with shCtrl (n = 18) or shSynGAP 3'UTR (n = 20) were immunostained

for MAP2 (red). F-actin (green) was stained by fluorescein-conjugated phalloidin. Scale bar = 5 μm . (K) Quantification of the number of spines per 1 μm and the percentage of mature spines in (J) (spine number: ***P < 0.001, Mann-Whitney U test; mature spines: ***P < 0.001, un-paired t-test). In (B), (E), (F), (I) and (K), data represent mean \pm SEM. See also Figure S3.

Figure 5. FUS regulates SynGAP α 2 mRNA with ELAV-like family proteins at the 3'UTR.

(A) Experimental schema of the biotinylated RNA pull-down assay using SynGAP mRNA 3'UTR sequences, followed by mass spectrometry analysis. (B) The RNA pull-down assay was performed by using a biotinylated RNA probe cloned from the SynGAP 3'UTR (see precise location in Figure S3). Pull-down samples were analyzed by western blotting with the indicated antibodies. (C) Quantification of the band intensity in (B) (*P < 0.05, un-paired t-test). (D) The lysates from primary cortical neurons infected with lentiviruses (shCtrl or shELAVL4, n = 3 each) were analyzed by western blotting with the indicated antibodies. (E) Quantification of the band intensity of the indicated proteins in (D) (normalized to GAPDH intensity; ***P < 0.001, **P < 0.01, un-paired t-test). (F) mRNA stability was measured in the control and ELAVL4 knockdown primary cortical

neurons as described in Figure 4B (n = 3) (*P < 0.05, ANCOVA). (G) RNA pull-down assay with SynGAP probes in ELAVL4 knockdown primary cortical neurons (n = 3). Bound proteins were analyzed by western blotting with the indicated antibodies. (H) Quantification of the band intensities in (G) (*P < 0.05, **P < 0.01, un-paired t-test). (I) Cultured cortical neurons were transduced with lentiviruses expressing shCtrl, shFUS, shELAVL4 and shFUS+shELAVL4 (n = 3 each). Total RNA was extracted and used for qRT-PCR with the indicated primers (***P < 0.001, one-way analysis of variance). (J) qRT-PCR of primary cortical neurons infected with shCtrl or shELAVL1 lentiviruses (n = 4 each) (**P < 0.01, ***P < 0.001 un-paired t-test). In (C), (E), (F), (H), (I) and (J), data represent mean \pm SEM. See also Figures S4.

Figure 6. FUS depletion causes spine and behavioral abnormalities that are ameliorated by SynGAP α 2 expression.

(A) The hippocampi of FUS fl/fl Cre- or FUS fl/fl Cre+ mice were immunostained with an FUS antibody. Scale bar: 200 μ m. (B) The CA1 region of the hippocampus from Cre- or Cre+ mice was excised and sonicated. The lysates were analyzed by western blotting with the indicated antibodies. (C) Quantification of the band intensity in (B). (normalized to GAPDH intensity; *P < 0.05, **P < 0.01, un-paired t-test). (D) The CA1 regions of the

hippocampi from Cre- or Cre+ mice were immunostained for SynGAP $\alpha 2$ (red), FUS (green), and DAPI (blue). Scale bar: 10 μm . (E) Golgi staining in the CA1 region of the hippocampus. FUS flox mice were injected with GFP or SynGAP $\alpha 2$ (n = 3 each). Scale bar: 10 μm . (F) The total number of spines per 100 μm of dendrite was quantified (NS = not significant, one-way analysis of variance) (G) The percentage of mushroom spines per 100 μm of dendrite was quantified (***P < 0.001, one-way analysis of variance). (H) Exploring distance in the open field test. Number of Cre-GFP/Cre+ GFP/Cre+ SynGAP $\alpha 2$ samples = 14 / 11 / 11 (total and outer arena: *P < 0.05, **P < 0.01, Kruskal-Wallis test; center arena: NS = not significant, one-way analysis of variance). (I-J) Results of the elevated plus maze test. Number of Cre-GFP/Cre+ GFP/Cre+ SynGAP $\alpha 2$ samples = 8 / 7 / 8. (I) Percentage of time in open arms compared with the total time in open plus closed arms (*P < 0.05, one-way analysis of variance). (J) Open arms entries were counted (*P < 0.05, one-way analysis of variance). In (C), (F), (G), (H), (I) and (J), data represent mean \pm SEM. See also Figure S5.

Figure 1

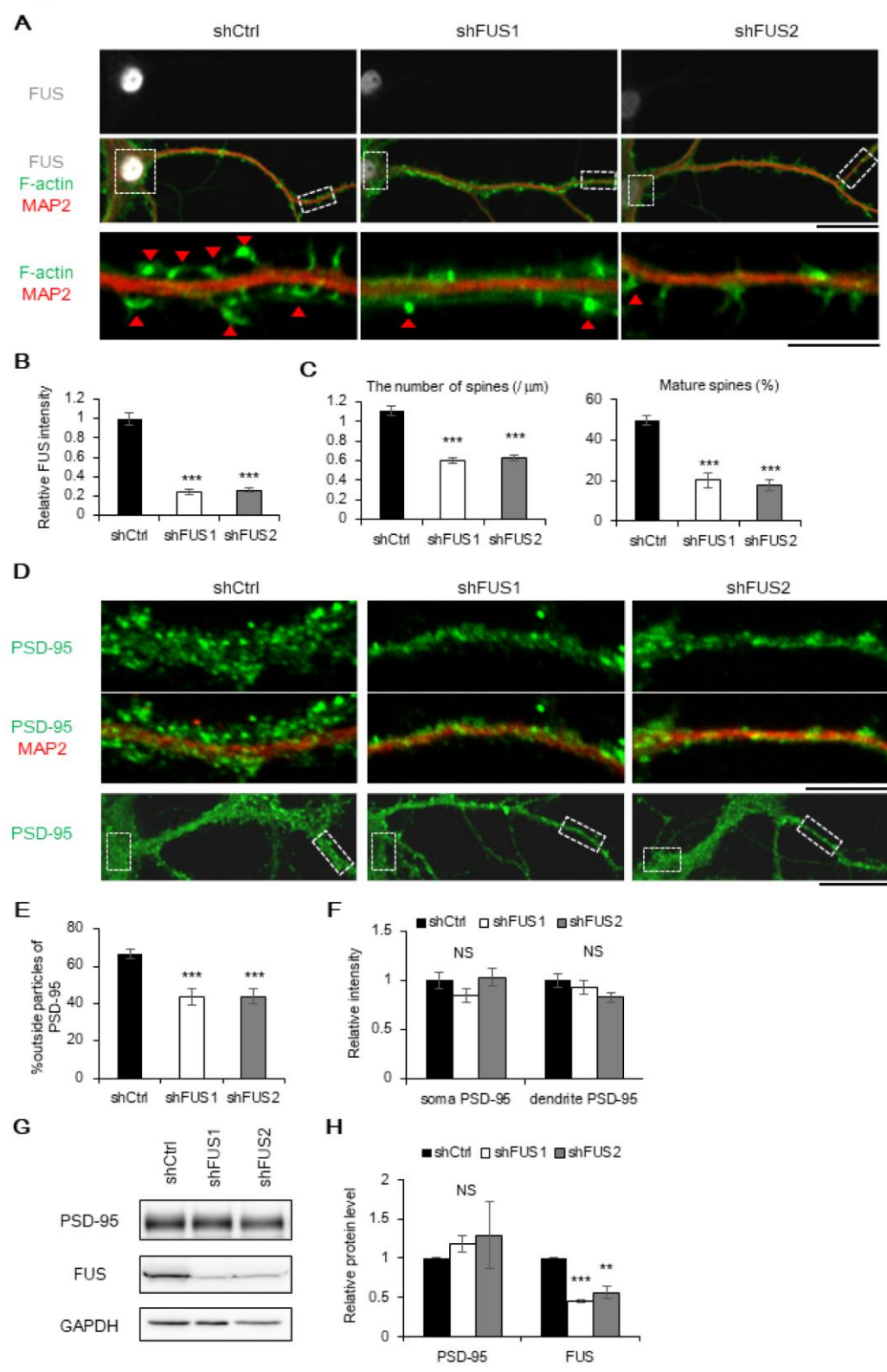
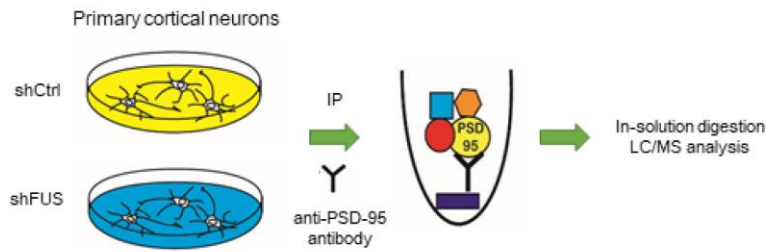
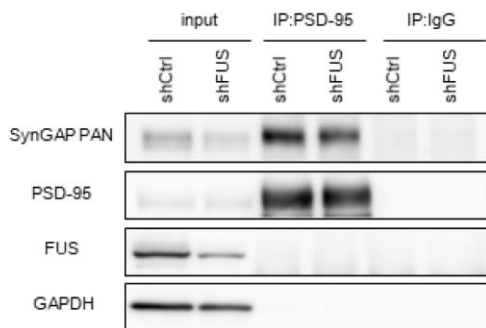


Figure 2

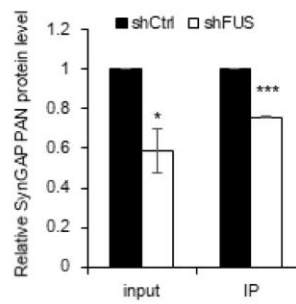
A



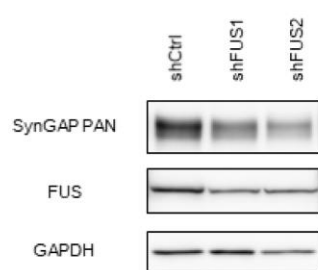
B



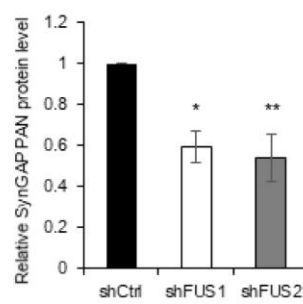
C



D



E



F

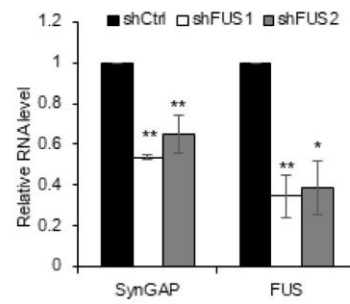


Figure 3

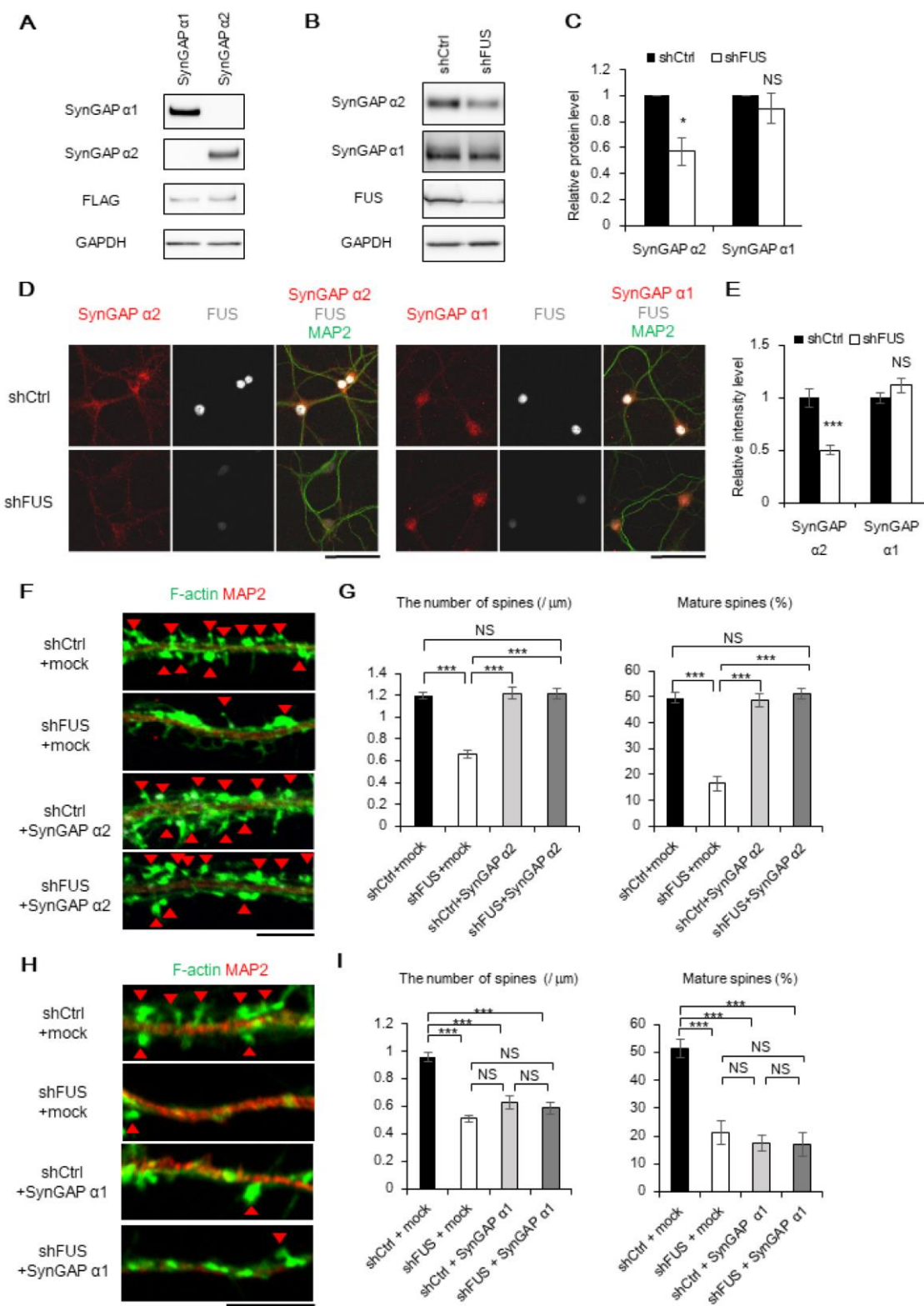


Figure 4

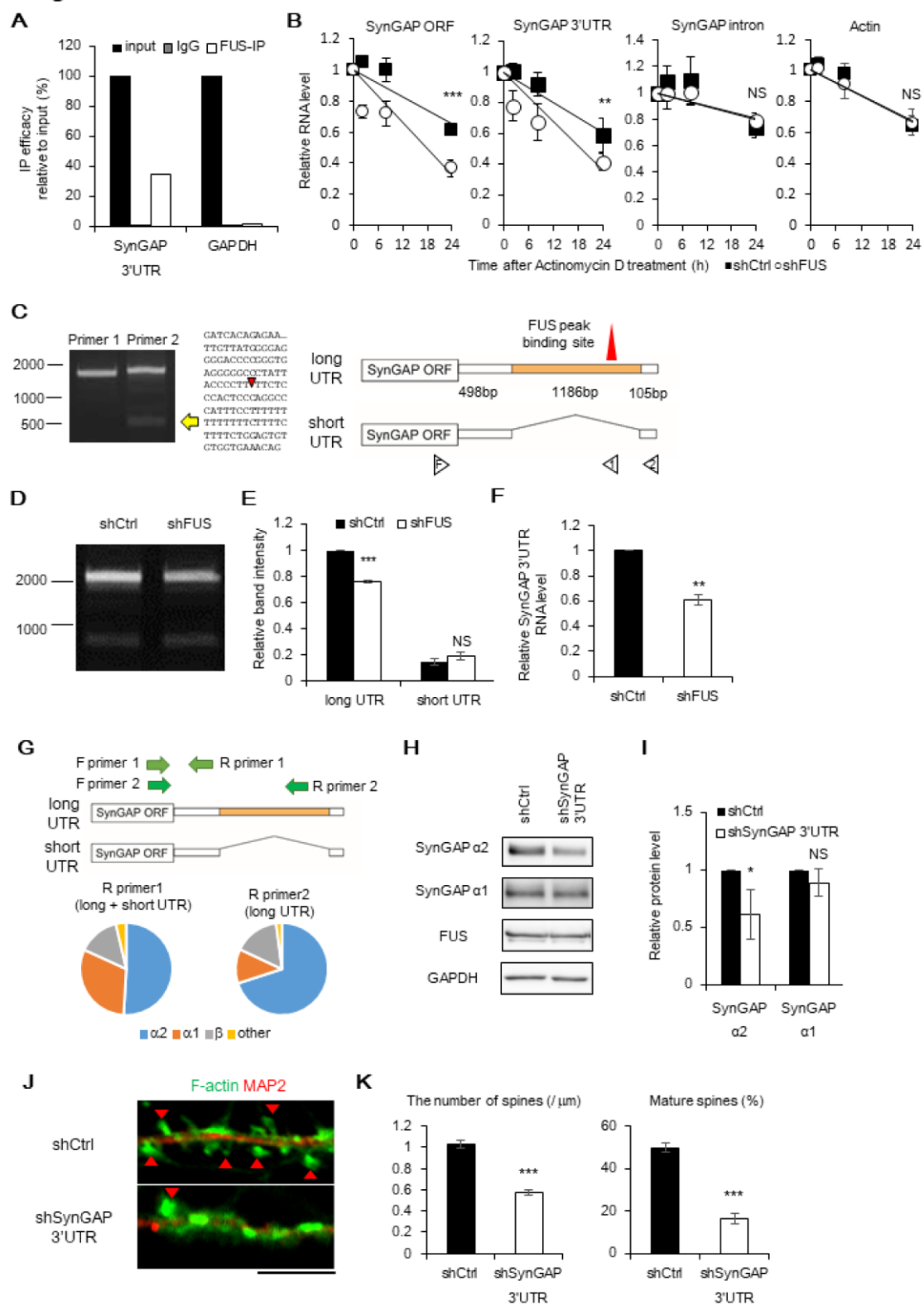


Figure 5

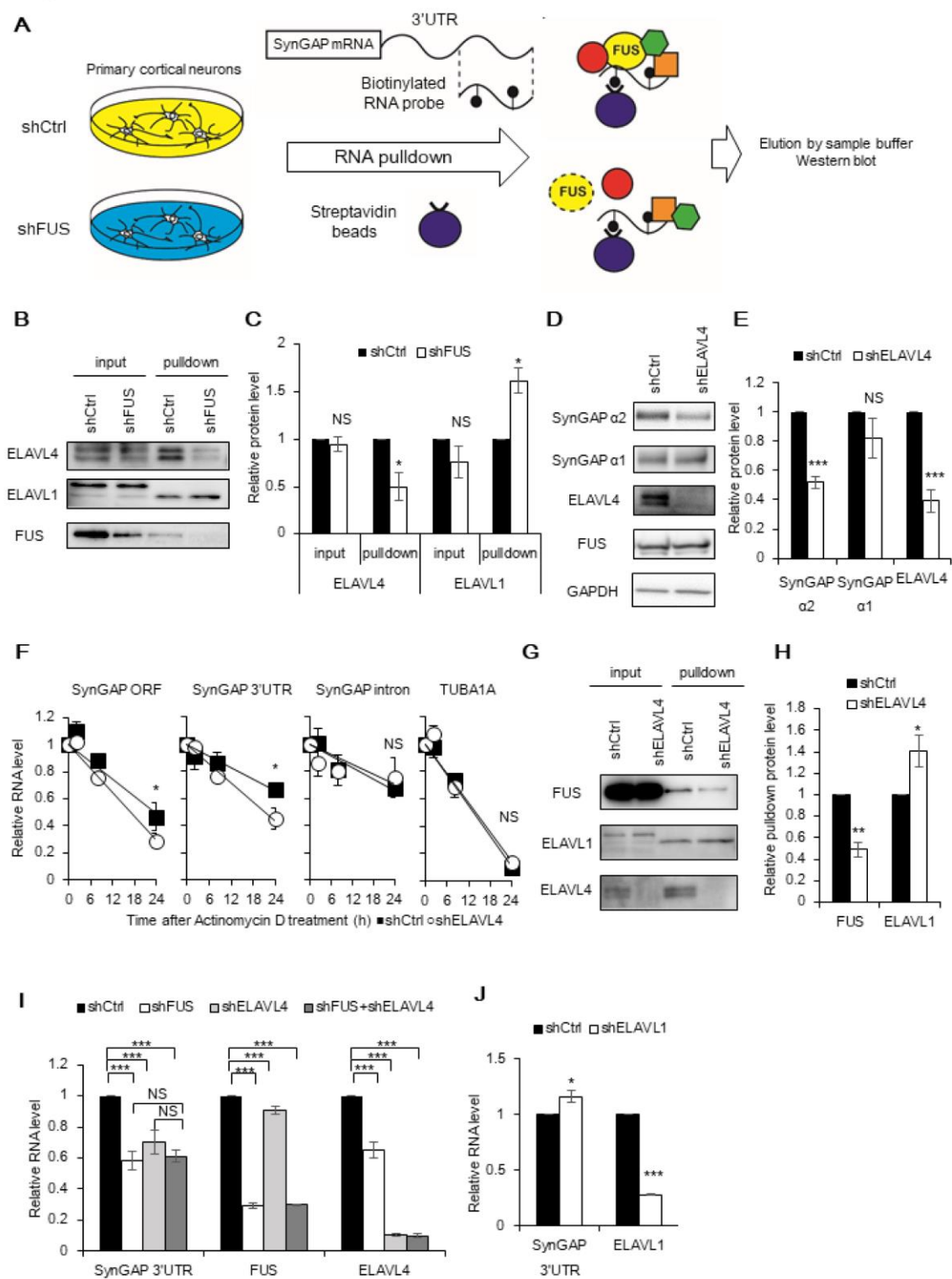


Figure 6

